BNL-228874-2025-TECH
EIC-ADD-TN-138

Hadron Storage Ring Transition Crossing for Yellow Only Configuration

H. Lovelace III

September 2025

Electron-Ion Collider Project

Brookhaven National Laboratory

U.S. Department of Energy

USDOE Office of Science (SC), Nuclear Physics (NP)

Notice: This technical note has been authored by employees of Brookhaven Science Associates, LLC under Contract No.DE-SC0012704 with the U.S. Department of Energy. The publisher by accepting the technical note for publication acknowledges that the United States Government retains a non-exclusive, paid-up, irrevocable, world-wide license to publish or reproduce the published form of this technical note, or allow others to do so, for United States Government purposes.

DISCLAIMER

This report was prepared as an account of work sponsored by an agency of the United States Government. Neither the United States Government nor any agency thereof, nor any of their employees, nor any of their contractors, subcontractors, or their employees, makes any warranty, express or implied, or assumes any legal liability or responsibility for the accuracy, completeness, or any third party's use or the results of such use of any information, apparatus, product, or process disclosed, or represents that its use would not infringe privately owned rights. Reference herein to any specific commercial product, process, or service by trade name, trademark, manufacturer, or otherwise, does not necessarily constitute or imply its endorsement, recommendation, or favoring by the United States Government or any agency thereof or its contractors or subcontractors. The views and opinions of authors expressed herein do not necessarily state or reflect those of the United States Government or any agency thereof.

Hadron Storage Ring Transition Crossing for Yellow Only Configuration

H. Lovelace III, S. Berg, K. Drees, G. Robert-Demolaize, S.Peggs, V. Ptitsyn, R. Seviour

September 8, 2025

Abstract The Electron Ion Collider (EIC) Hadron Storage Ring (HSR) has undergone many iterations. This technical note captures the progress made on transition crossing in the HSR studies for the yellow only configuration. Being heavily dependent on the phase advance per cell, the `hsr-au-trans-8786phi-071725` optics was used where the phase advances per arc cell are 87°, horizontal and 85°, vertical. These phase advances were chosen to aid in the cancellation of the β and η waves generated during the jump and to minimize the tune shift. The total change in the γ_T is 1 unit as prescribed by [1]. This technical note will describe the process in which HSR will jump transition with the assumption that longitudinal dynamics will be handled similar to the Relativistic Heavy Ion Collider (RHIC) [2].

1 Introduction

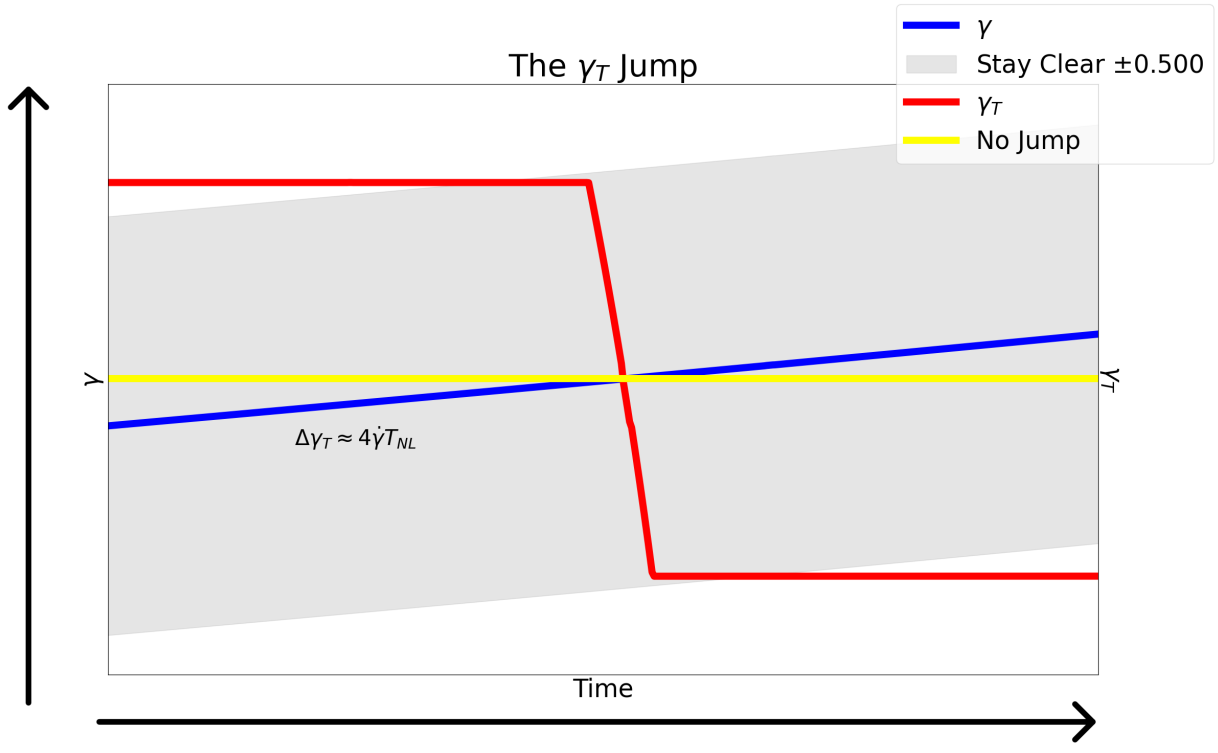


Figure 1: A schematic of the transition jump of -1 unit. The blue curve is the increase of energy through transition where the yellow curve is the γ_T without the jump and the red curve is γ_T with the jump. The "stay clear" region is marked in gray with the formula for the region.

The Hadron Storage Ring (HSR) will use the Relativistic Heavy Ion Collider (RHIC) tunnel and reuse the majority of the RHIC yellow ring magnets. While the arcs are preserved, the insertion regions (IR) are rearranged with the exception of IR2 and IR6 being fully replaced. Due to the complexity of the optics in the refurbished IRs, the placement of the γ_T quadrupoles destroys the symmetry of the First Order Matched (FOM) that is used in RHIC. In the FOM the change in γ_T of the lattice is linear to the integrated normalized strength of the i^{th} jump quadrupole:

$$\Delta\gamma_T = \frac{\gamma_T^3}{2C_0}\sum_i (k_1 l)_i \eta_i^2 \tag{1}$$

Where γ_T is the transition γ, C_0 is the circumference of the lattice, $(k_1 l)_i$ and η_i is the integrated normalized strength and dispersion of and at the i^{th} jump quadrupole. Figure 2 is the FOM when applied to the RHIC lattice. The

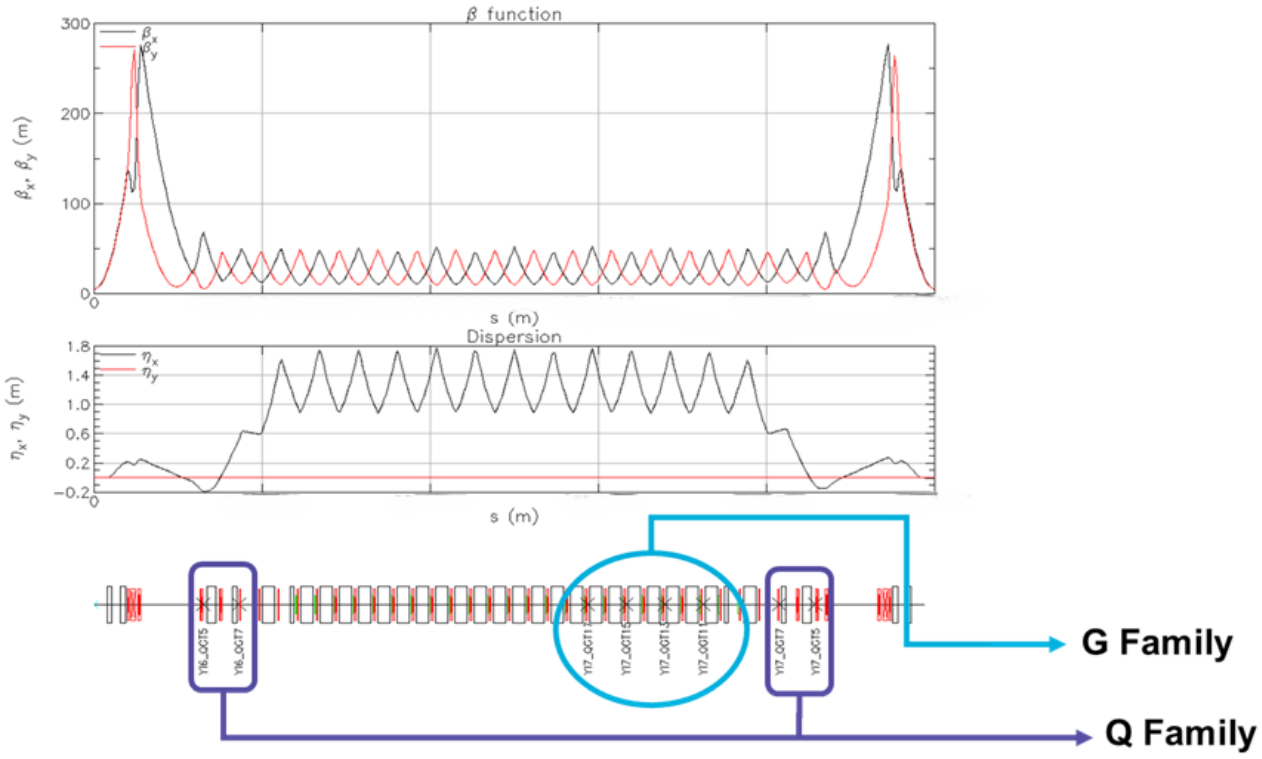


Figure 2: The FOM when applied to a typical sextant of RHIC. The circled G-family jump quadrupoles are in the dispersive section and the pair of doublets that surround the arc, Q-family, are in absolute minimal dispersive areas.

scheme is designed to correct the local tune shift and wave generation driven by the arc jump quadrupoles. The lattice defined γ-transition, γ_T, is a direct feature of a closed geometry periodic lattice that at transition energy, affects the particle bunch by decreasing the bunch length and simultaneously increasing the momentum spread. This feature also forces the synchrotron tune to approach zero which causes the particle beam motion to become unstable [3]. Above transition, a particle given an accelerating kick by the RF will have a longer revolution period than a decelerating particle which will have a shorter period which is counter intuitive, as though the particle mass less than 0. A negative mass instability occurs when the density of the bunch increases with the decrease of the frequency spread at transition. Space charge detuning occurs at transition due to the minimization of the bunch length. These adverse effects from transition require that we move as quickly as possible through transition and since we are limited by the ramping speed of the main dipole magnets, we distort the optics of the lattice. The Lorentz factor at transition,

$$\gamma_T = 1/\sqrt{\alpha_0} \tag{2}$$

, where the momentum compaction, α_0

$$\alpha_0 = \oint ds(\eta_x/\rho_x) \tag{3}$$

The quantities η_x and ρ_x, horizontal dispersion and radius of curvature are gathered from the electromagnetic lattice of the accelerator. We define the slippage as, η_s:

$$\eta_s = \alpha_0 - 1/\gamma^2 \tag{4}$$

where if $\eta_s < 0$ the particles that are more energetic than the synchronous will have a shorter revolution period, and if $\eta_s > 0$ the particles that are more energetic than the synchronous will have a longer revolution period therefore at transition the revolution period of the particle is independent of the particle's energy. When $\eta_s = 0$, the beam is at the lattice transition energy.

The G-family, which is the quadruplet of quadrupoles in the arc, distorts the optics and dispersion when excited in such a way that the γ_T of the lattice becomes dynamic and for HSR, this is a change of ± 0.5 units. The Q-family, which are pairs of doublets that reside around the arc in minimum dispersion areas, compensate for the tune shift driven by the G-family by ramping with the opposite polarity. To optimize the effectiveness of the jump quadrupoles, the β-functions at the jump quadrupoles must be identical and the jump quadrupoles must be separated by a phase advance of 90°.

The current HSR (git #ef2e8c3 for reference), breaks the symmetry of the standard RHIC layout with the redesign of IR2 and IR6. Figure 3 shows the layouts of RHIC and the HSR. RHIC contains 24 G-family jump

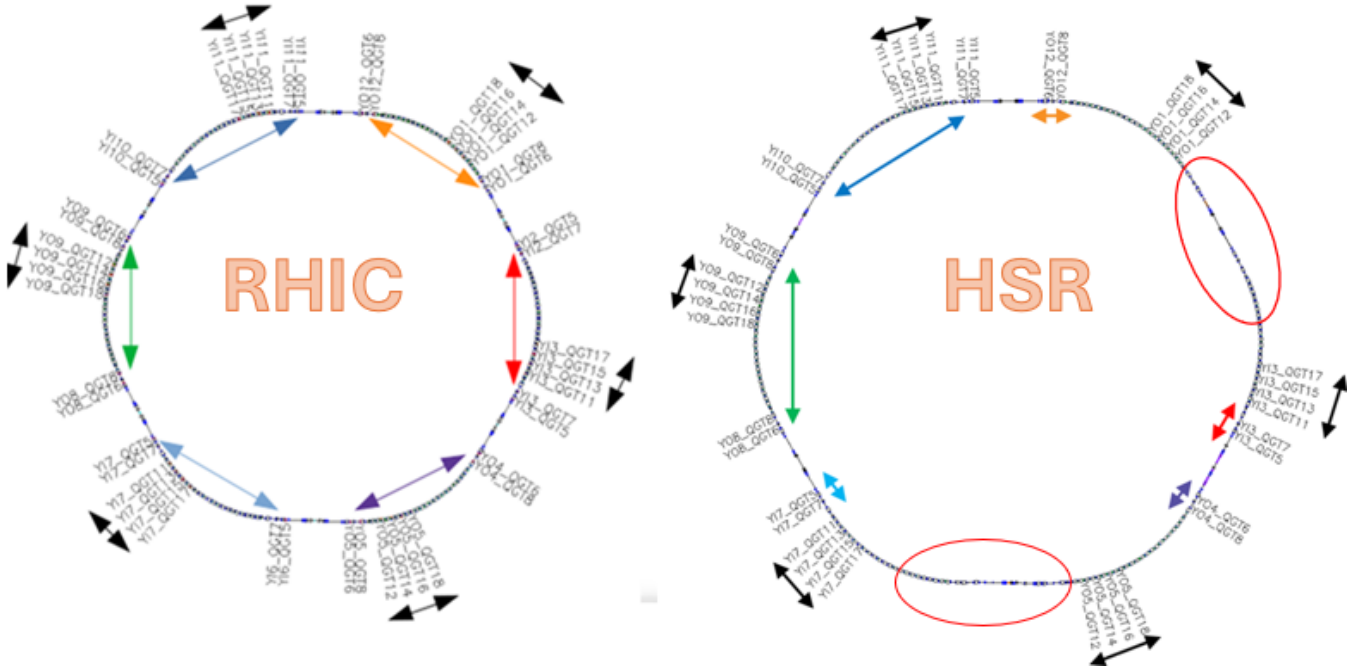


Figure 3: A comparison of the jump quadrupoles placement in RHIC and the HSR. The number of jump quadrupoles in RHIC is 48 where there are 24 jump quadrupoles for the G-family and 24 jump quadrupoles for the Q-family. The HSR has 24 G-family jump quadrupoles of 16 Q-family jump quadrupoles that are in the correct placement and phase advance.

quadrupoles and 24 Q-family jump quadrupoles (G24Q24) whereas the HSR contains 24 G-family, and 16 Q-family jump quadrupoles (G24Q16). For the HSR, 16 Q-family quadrupoles are not evenly spread throughout the lattice. The standard FOM scheme is broken for the arcs adjacent to IRs 2 and 6. This presents a challenge in the minimization of the wave generation when the jump quadrupoles are at their peak excitation.

2 Formulating the γ_T Jump

The dependency on the slippage causes the synchrotron tune/frequency) to slow to zero as transition is approached and the adiabaticity condition,

$$\Omega = \frac{1}{\omega_s^2}\left|\frac{d\omega_s}{dt}\right| \ll 1 \tag{5}$$

where ω_s is the angular frequency and t is time, ceases to be satisfied [4]. In Equ. 5, it is clear that there is no change in the action provided that $\Omega \ll 1$ [5]. The nonadiabatic or characteristic time, T_c, during which the beam loses its adiabaticity is

$$T_c = \left(\frac{AE_T}{ZeV|\cos(\phi_s)|} \times \frac{\gamma_T^3}{h\gamma'} \times \frac{C_0^2}{4\pi c^2}\right)^{1/3}, \tag{6}$$

where A is the atomic weight, Z is the atomic number, E_T is the transition energy, e is the charge of the electron, V is the RF cavity voltage, γ_T is the transition γ, h is the harmonic number, and $\gamma' = d\gamma/dt$.

The Johnsen time [6] in which the particles within a bunch with a given momentum spread experience transition is

$$T_{NL} = \left(\alpha_1 + \frac{3}{2}\beta_T^2\right)\frac{\gamma_T}{\gamma'}\delta_{max}, \tag{7}$$

where β_T is the velocity ratio of the beam centroid, $\delta_{max} = \Delta p_{max}/p$ is the maximum momentum spread of the bunch, and α_1 is the "nonlinear momentum compaction factor" defined by [7]

$$\delta C/C_0 = \alpha_0\delta(1 + \alpha_1\delta + ...), \tag{8}$$

where C is the path length of the beam and C_0 is the circumference of the lattice. If $\alpha_1 = -1/2$, all particles within the bunch have the same γ_T. For all particles to cross transition at the same time, $\alpha_1 = -3/2$. The maximum momentum spread of the beam at transition can be written as [8],

$$\delta_{max} = \frac{\omega_s\sqrt{2hSqe\hat{V}|\cos\phi_s|T_c}}{\sqrt[3]{9}\sqrt{\pi}\Gamma(2/3)AE_0\beta_s^2}, \tag{9}$$

where $\hat{V}$ is the peak accelerating voltage, h is the cavity harmonic, ϕ_s is the synchronous phase, AE_0 is the total energy of the particle, A is the atomic number, β_s the velocity ratio, and qe is the charge of the particle. The $\Gamma(2/3)$ is approximately 1.3541.

A "stay clear" area is needed to safely cross transition if the nonlinear time is much greater than the characteristic time, $T_{NL} \gg T_c$

$$\Delta\gamma_T \approx 4\dot{\gamma}T_{NL}. \tag{10}$$

to prevent unwanted detrimental effects of off-momentum particles crossing transition too early or late. Figure 1 is a schematic of change in γ_T with respect to time with a jump and without a jump. The jump duration is 40 ms which in HSR is approximately 3300 turns. During the jump the γ_T value changes by -1 unit.

S is the RMS bunch area [9] before transition which effective increase can be formulated as [10]

$$\frac{\Delta S}{S} = \begin{cases} 0.76\frac{T_{NL}}{T_c} & \text{for } T_{NL} \ll T_c \\ e^{4/3(\frac{T_{NL}}{T_c})^{3/2}} - 1 & \text{for } T_{NL} \geq T_c \end{cases}. \tag{11}$$

Space charge, an intensity dependent collective effect where the particle field acts upon its neighbor within the bunch, becomes prevalent during transition due to the decrease in bunch length. The peak current is

$$\hat{I} = \frac{3hN_0qew_s}{4\hat{\phi}}, \tag{12}$$

where N_0 is the intensity per bunch. The maximum phase spread is,

$$\hat{\phi} = \sqrt[6]{3}\Gamma(2/3)\sqrt{\frac{2hS}{\pi qe\hat{V}|\cos\phi_s||T_c}}. \tag{13}$$

The β-beat and η-wave at the peak absolute excitation of the jump quadrupoles can be written as [11]

$$\begin{aligned}\frac{\Delta\beta_H}{\beta_H} =& \frac{1}{2\sin(2\pi Q_H)} \\ & \sum_i (k_1 l)_i \beta_{Hi} \cos(2|\phi - \phi_i| - 2\pi Q_H)\end{aligned} \tag{14}$$

and

$$\begin{aligned}\frac{\Delta\eta}{\sqrt{\beta}} =& \frac{1}{2\sin(\pi Q_H)} \\ & \sum_i (k_1 l)_i \eta_i \sqrt{\beta_{Hi}} \cos(|\phi - \phi_i| - \pi Q_H)\end{aligned} \tag{15}$$

where the difference in phase advance $\Delta\phi = |\phi - \phi_i|$ is taken at the jump quadrupole from a phase advance upstream of the doublet or quadruplet.

2.1 Jump Quadrupole Sensitivities, Strength Ratio, k

The relationship between the strengths of the two jump quadrupole types, G and Q, is [1, 12]:

$$q_G = k q_Q \tag{16}$$

where k is the proportionality constant that relates the integrated normalized strength, q_Q, of the Q family to the integrated normalized strength, q_G, of the G family. The value of k is determined by sensitivities associated with the jump quadrupole families. The sensitivities, $S_{G,p}, S_{Q,p}$ are summed over the jump quadrupoles of each power supply, p.

$$\begin{aligned}S_{G,p} &= \frac{\gamma_{T0}^3}{2C_0} \sum_p \eta^2 \\ S_{Q,p} &= \frac{1}{4\pi} \sum_p \beta_H .\end{aligned} \tag{17}$$

The sensitivities are found at both the G and Q families producing four numbers, $G(S_{G,p}, S_{Q,p})$ and $Q(S_{G,p}, S_{Q,p})$. A response matrix, T, that is used to obtain the G-family to Q-family ratio, can be obtained from these sensitivities

$$T = \begin{pmatrix} T_{GG} & T_{GQ} \\ T_{QG} & T_{QQ} \end{pmatrix} = \begin{pmatrix} \sum S_{G,p}^G & \sum S_{G,p}^Q \\ \sum S_{Q,p}^G & \sum S_{Q,p}^Q \end{pmatrix}. \tag{18}$$

The ratio of the $(-T_{QG}/T_{QQ}) = k$.

2.2 Jump Quadrupole Sensitivities, β- and η-waves

Other metrics that are used in determining the effectiveness of the jump quadrupoles are the sensitivities to the phase advance within a given jump quadrupole family. Derived from Equ. 14 and 15, we may write the sensitivity to the β- and η-wave generation, S_{bw} and S_{hw} as:

$$S_{bw} = \frac{\Delta\beta_H}{\beta_H}/(k_1 l)_i = \frac{\beta_{Hi}\cos(2|\phi - \phi_i| - 2\pi Q_H)}{2\sin(2\pi Q_H)} \tag{19}$$

and

$$S_{hw} = \frac{\Delta\eta}{\sqrt{\beta}}/(k_1 l)_i = \frac{\eta_i\sqrt{\beta_{Hi}}\cos(|\phi - \phi_i| - \pi Q_H)}{2\sin(\pi Q_H)} \tag{20}$$

From S_{bw} and S_{hw}, it is clear to see that the difference in the phase advance of the jump quadrupoles increases the wave sensitivities as the phase advance moves away from 90°. To better illustrate the point, Fig. 4 shows the effect of the increasing difference in the phase advance from 75° to 90°.

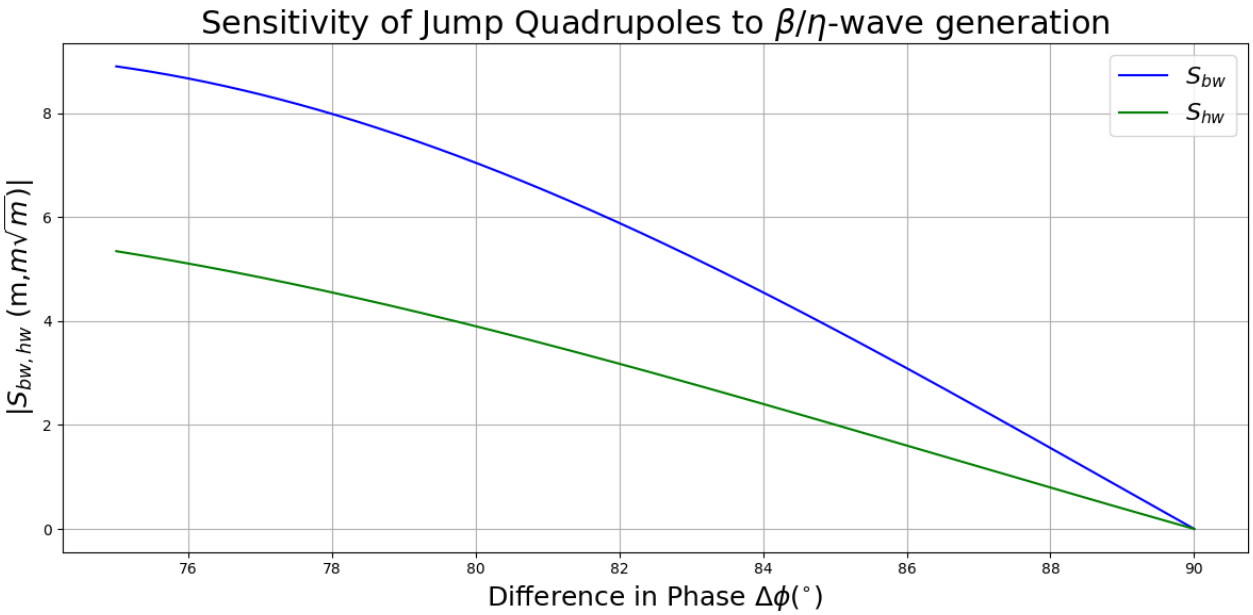


Figure 4: The sensitivities S_{bw} and S_{hw} absolute value decreases as the phase advance moves closer to 90°. For S_{bw} doublets are considered and for S_{hw} quadruplets

3 Hadron Storage Ring Optics

The HSR transition optics with a cooling IR2 layout, shown in Fig. 5, are designed to place the phase advance per cell in the arcs as close to 90° as possible while constraining γ_T below the γ needed for hadron beam cooling. The beam direction in plot is from right to left, counterclockwise in the HSR. The horizontal β^* of IR4 IR6, IR8, IR10, and IR12 is 5 m with IR6 having a vertical β^* of 1 m while the IR4, IR8, IR10, and IR12 vertical β^*s equal 5 m. The optics of IR2, located between s approximately 2400 to 2700, at transition maintain a relatively flat β-function and fully suppress dispersion for cooling purposes. The injection region, IR4, maintains the triplet optics of RHIC however, the dipole layout has changed. The warm dipoles that are the final bend before the midpoint of the IR in the RHIC-like IRs (IR8, IR10, and IR12) are between the triplets whereas in IR4 the downstream warm dipoles are located downstream of the second set of triplets in the IR. They not only set the geometry of the lattice but also are used as spectrometer dipoles for tagging particle fragments generated by the polarization jets in the IR. Table 1 gives that parameters associated with transition lattice (trans-ef2e8c3:hsr-au-trans-8786phi-071725.var) **without** and **with** a transition jump. During the jump only the transition quadrupoles are excited to distort the optics of the lattice.

3.1 HSR with G24Q16-cool Configuration

Without introducing additional jump quadrupoles in IR2 or IR6, the performance through transition will suffer due to increased β-beating which causes scraping in the apertures of the magnet. The reduction of jump quadrupoles allow the β-wave to propagate around the ring. Table 8 shows the various sensitivities discussed in Equs. 14, 15, 19, and 20 for the existing jump quadrupoles and the sum of the sensitivities on a given power supply. From the S_G and S_Q power supply columns, the ratio of the strengths of the G and Q, Equ. 16, are found to be $k_{inner} = -1.24$ and $k_{outer} = -1.61$ where inner and outer denote the position of the arc. The wave sensitivities show that at 87° the arc sensitivity remains close to zero while the straight section jump quadrupoles have great influence on the β-wave generation.

The horizontal tune before the jump is 28.226 and the vertical is 29.235. After the jump, the tunes are 28.209 and 29.227, horizontal and vertical, respectively. The post jump horizontal tune is close to the 5^{th} order betatron tune, 0.2 fractional, which can cause beam loss when crossed. The wave generation for the G24Q16-cool configuration is shown in Fig. 6 where Fig. 6a is the pre-jump wave generation and Fig. 6b is the post-jump. The currents

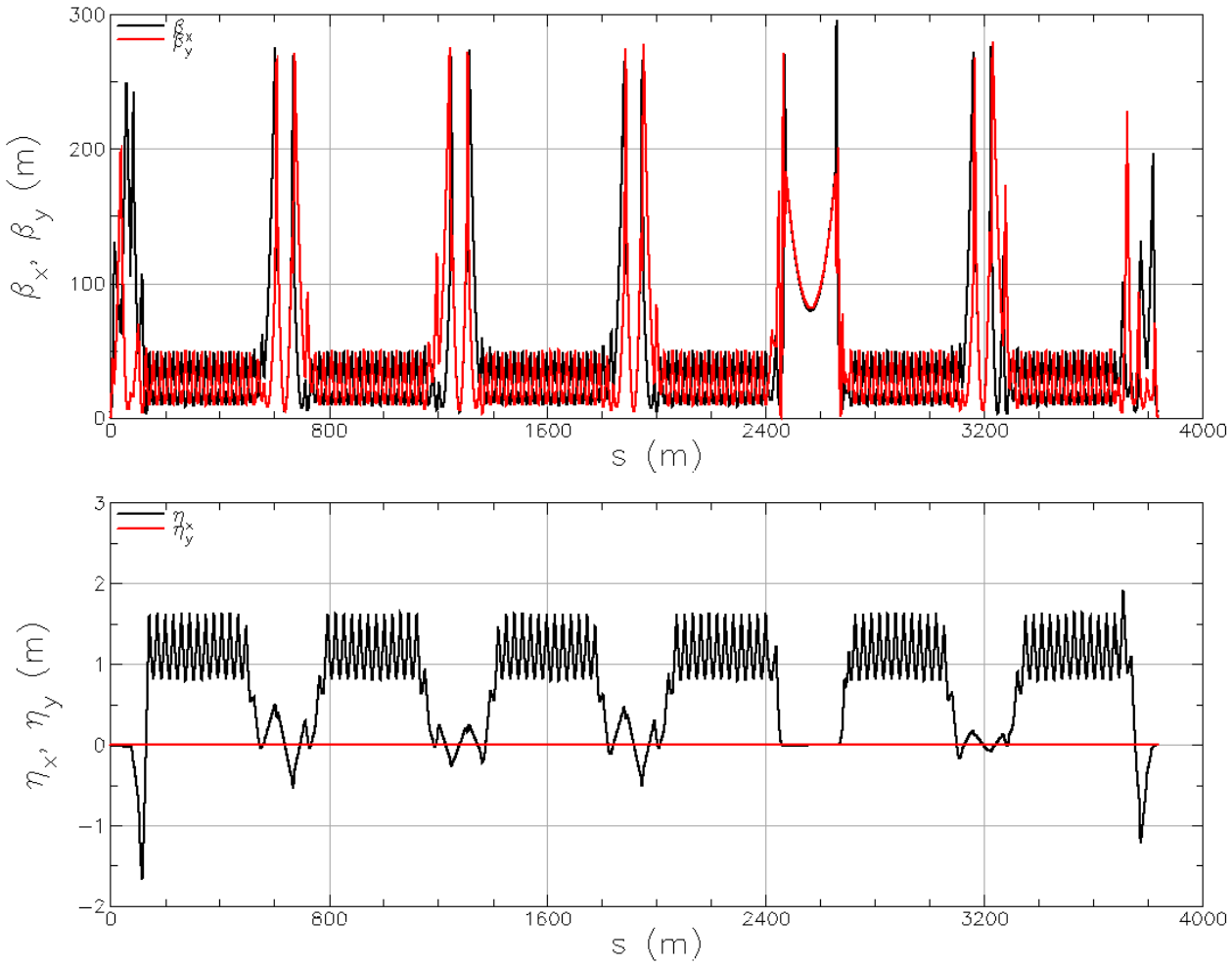


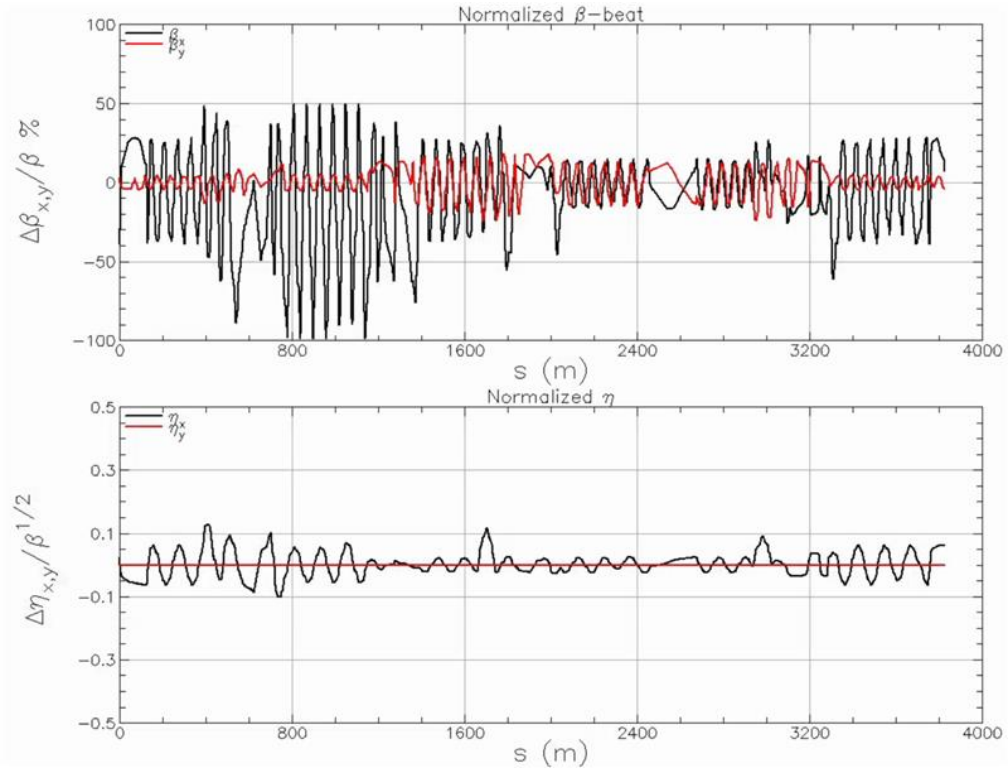
Figure 5: The HSR transition optics with a cooling IR2 layout starting at IP6 with increasing s clockwise. The beam direction is from right to left in the two plots. Top: Twiss parameters with black the horizontal plane and red the vertical plane. Bottom: Dispersion with black the horizontal plane and red the vertical plane.

of the four families are in Tab. 2.

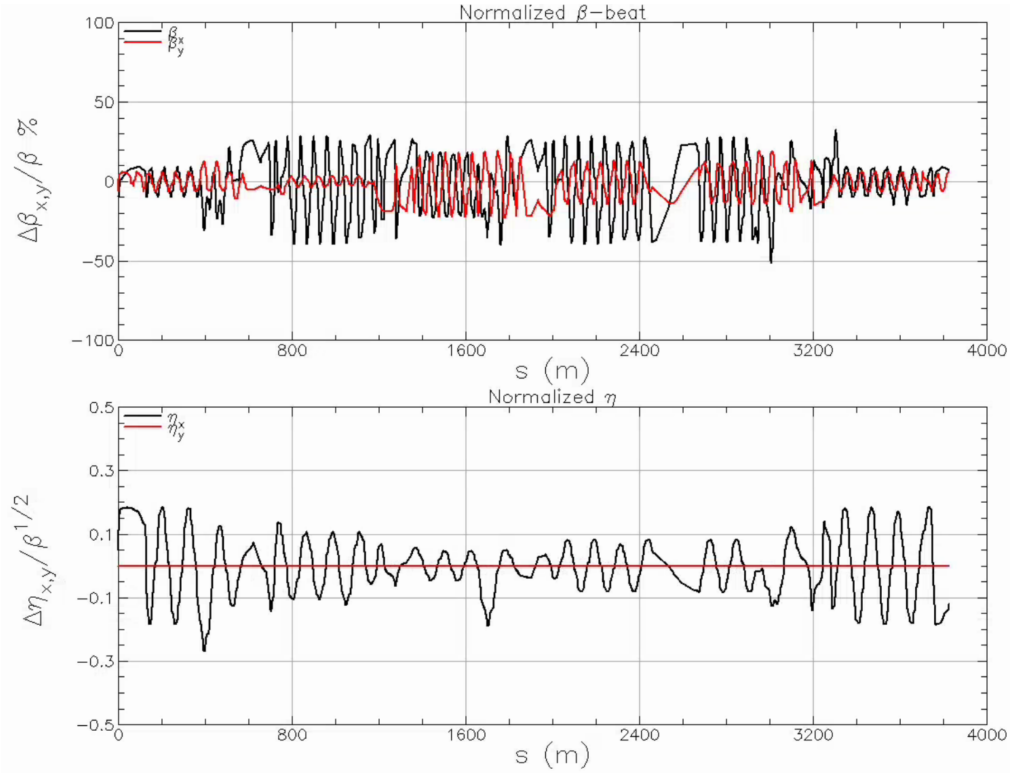
The transfer function of the jump quadrupoles is 0.03065172 Tm/A which means that at 47 A the maximum field needed for the jump is $0.8{\times}10^{-3}\,m^{-1}$. Due to lattice symmetry breakage, the k_{inner} and k_{outer} values greatly differ from the optimal values which are $k_{inner} = k_{outer} = 1$.

3.2 HSR with G24Q20-cool Configuration

The G24Q20-cool configuration introduces jump quadrupoles in the IR6 region. Though the phase advances and dispersion do not meet the standard requirement for the γ_T jump quadrupoles, the quadrupoles are used for tune compensation. These quadrupoles help driving the post-jump working point away from strong resonances. Due to space constraints inherent to the full reworking of IR6, it is a challenge to find empty slots available for these extra jump quadrupoles. The γ_T jump quadrupoles use corrector packages associated with IR quadrupoles and in IR6 slot for the jump quadrupoles are in competition with the skew quadrupoles. The tune is better controlled through the polarity flip of the jump quadrupoles with the additional 4 jump quadrupoles IR6. The pre-jump horizontal tune is 28.221 and the vertical tune is 29.213. The post-jump tunes are 28.215 and 29.213, horizontal and vertical, respectively. Figure 13 shows the change in $\Delta Q_{h,v}$, $\beta_{max\,x,y}$, $\Delta\gamma_T$, and $\eta_{max\,x,y}$. The wave generation for the G24Q20-cool configuration is shown in Fig. 9 where Fig. 9a is the pre-jump wave generation and



(a) The pre-jump wave generation. Top: β-wave with black curve horizontal and red vertical wave. Bottom: β-wave with black curve horizontal and red vertical wave.



(b) The post-jump wave generation. Top: β-wave with black curve horizontal and red vertical wave. Bottom: β-wave with black curve horizontal and red vertical wave.

Figure 6: The wave generation during the transition jump of the G24Q16 cooling configuration.

Table 1: Nonadiabatic and nonlinear parameters necessary to determine transition crossing efficiency in the HSR. The second value is with a 40 ms jump.

Parameter	**Value**
Circumference, C [m]	3833.802
Bunch Intensity, [10^9]	2.0
Atomic Weight, A	196.97
Atomic Number, Z	79
Transition Energy, E_T [GeV]	24.58
Lattice Fractional Tunes $Q_{x,y}$	0.235, 0.232
RF Voltage, [kV]	200
Stable Phase, ϕ_s [rad]	0.074
Gamma Transition, γ_T	24.6
Harmonic Number, h	315
γ' [s^{-1}]	0.5
Bucket Area [eVs],	2375.90
Bunch Area [eVs],	66.79
Nonlinear factor, α_1	-5.4$\times 10^{-4}$
Nonadiabatic Time, T_c [ms]	71, 19
Nonlinear Time, T_{NL} [ms]	356, 4
Maximum Momentum Spread, δ_{max}	0.0041, 0.0025
Emittance Growth $\Delta S/S$,	3342904.74, 3.94
Maximum Phase Spread [°],	10.227, 19.629
Peak Current, [A]	16.448, 8.567

Jump Quadrupole PS	Current (A)
GTI	47
QTI	30
GTO	6
QTO	43

Table 2: The power supply absolute value of the peak current for G24Q16-cool transition jump configuration. The current has been rounded to the nearest amp.

Configuration	**G24Q16-Pre**	**G24Q20-Pre**	**G24Q16-Post**	**G24Q20-Post**
Hor. β-wave RMS	0.2876	0.2171	0.1804	0.2217
Ver. β-wave RMS	0.0894	0.1102	0.0922	0.0986
Hor. η-wave RMS ($\sqrt{m}$)	0.0393	0.0752	0.0888	0.1332

Table 3: β- and η-wave RMS values.

Fig. 9b is the post-jump. The currents of the jump quadrupole families are listed in 4

Table 3 shows a comparison of the RMS values of the wave generation between the two configurations, G24Q16-cool and G24Q20-cool. The G24Q16 columns show that pre-jump β-wave has a 40% increase compared to the post-jump wave RMS value and a 25% increase compared to the G24Q20-cool pre-jump lattice. The increase and a tune shift of 0.02 horizontally places the G24Q20-cool as a better configuration for transition crossing necessitating the use of jump qadrupoles in IR6.

3.3 HSR with G24Q20-nocool Configuration (RHIC-like IR2)

If the HSR construction plan is to maintain a RHIC-like IR2 and introduce cooling after first collisions of the EIC,the baseline lattice layout of the HSR will maintain the two pairs of Q-family doublets in IR2. Figure 10, version e74404c of the HSR, shows the Twiss parameters of the lattice with a RHIC-like IR2. The working point of

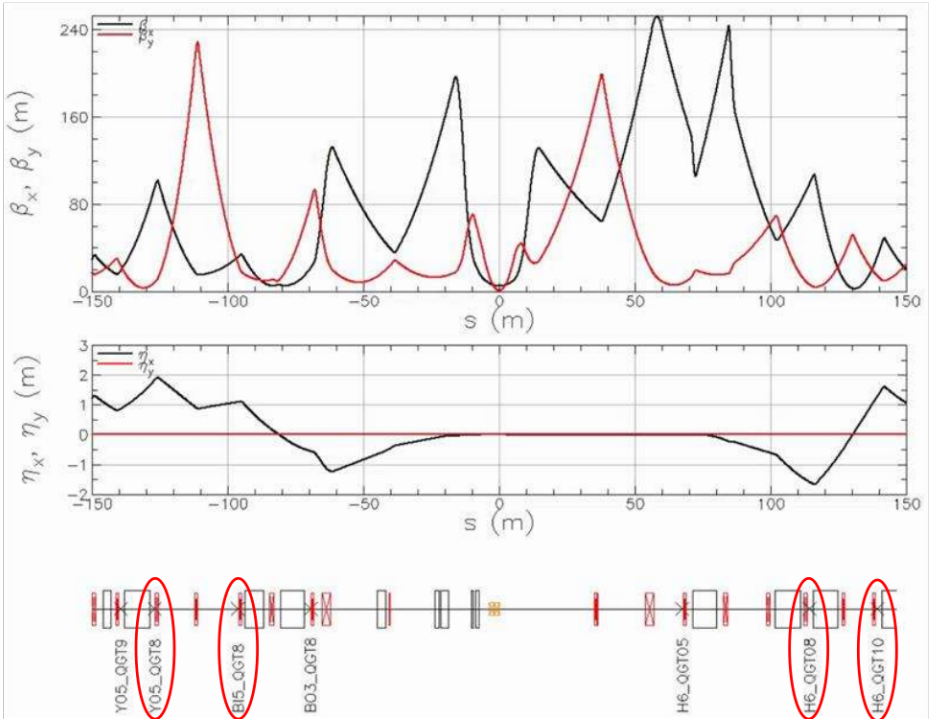


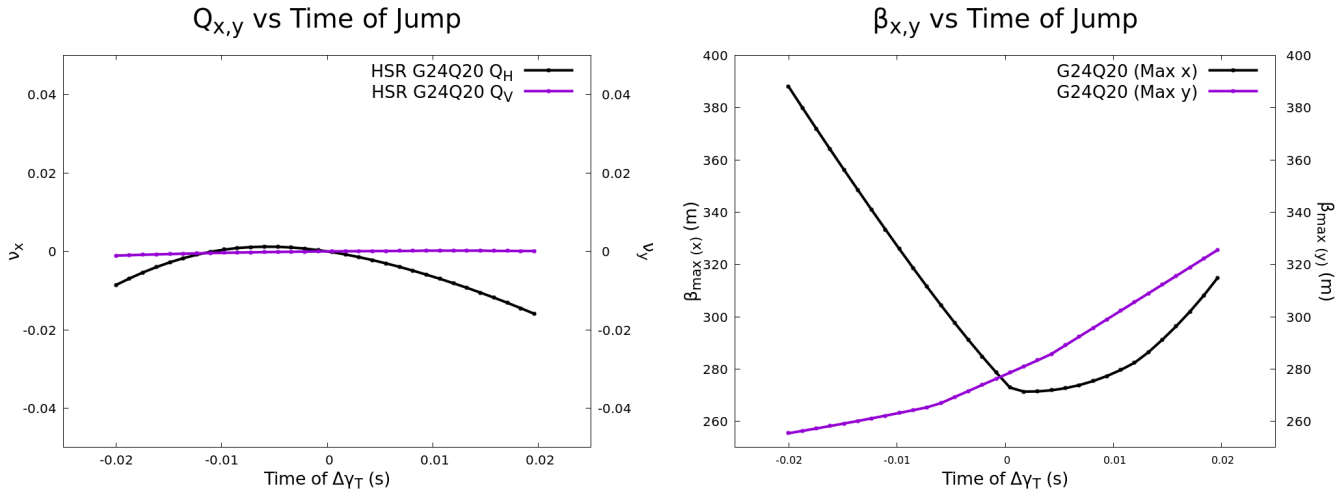
Figure 7: IR6 optics centered about IP6. Top: β-functions with black curve are horizontal plane and red curve is the vertical plane. Middle:η-functions with black curve is horizontal plane and red curve is the vertical plane. Bottom: Layout shows the possible jump quadrupole placement with the red circled locations used in the Fig. 9 configuration.

Jump Quadrupole PS	Current (A)
GTI	47
QTI	30
GTO	6
QTO	43
QTF3	-14
QTF5	-35
QTR8	-21
QTR10	-23

Table 4: The power supply absolute value of the peak current for G24Q20-cool transition jump configuration. The current has been rounded to the nearest amp.

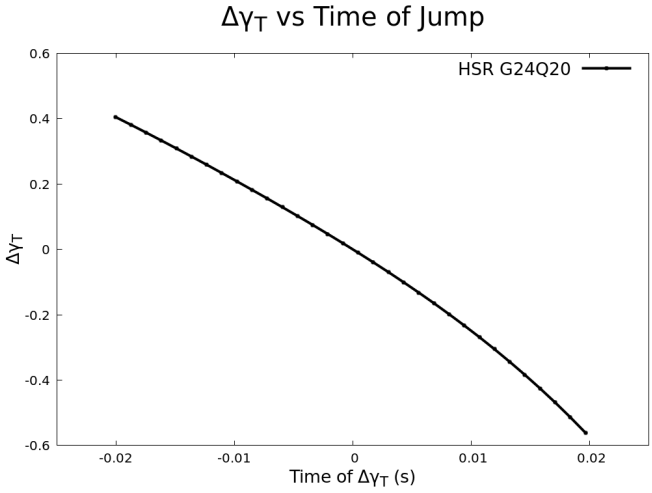
the lattice is 30.235 and 29.232, horizontal and vertical, respectively. The increase of two units of horizontal phase advance is a result of the phase advance difference in the non-cooling IR2 from the cooling IR2. The arc phase advance per cell is 87.5°, horizontal and 87.0°, vertical. The β^*s of the RHIC-like IRs is 5 m in both planes while IR6 maintains the 5 m horizontal and 1 m vertical β^*. The sensitivities at each jump quadrupole and for each family of jump quadrupoles are shown in Tab. 9. The addition of the four jump quadrupoles in IR2 has increased the ability to compensate for the tune shift and β-wave reduction as shown by the increase of the absolute sensitivities when compared to Tab. 8.

Figure 11 shows the waves generated once the jump quadrupoles are excited to their absolute value of the peak current. The β-waves in both planes are clearly more behaved than in Fig. 9. The slight residual waves generated are due to the lattice phase advance per cell having a 3° offset from the optimal value and the missing doublet in IR6. The RMS values of the waves are found in Tab. 6. With the increase in symmetry within the HSR, the currents of the jump quadrupoles become more balanced when compared to the cooling lattice. The currents

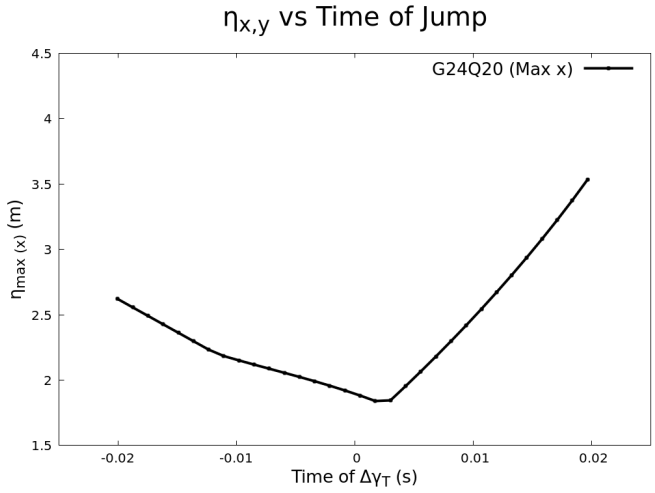


(a)

(b)

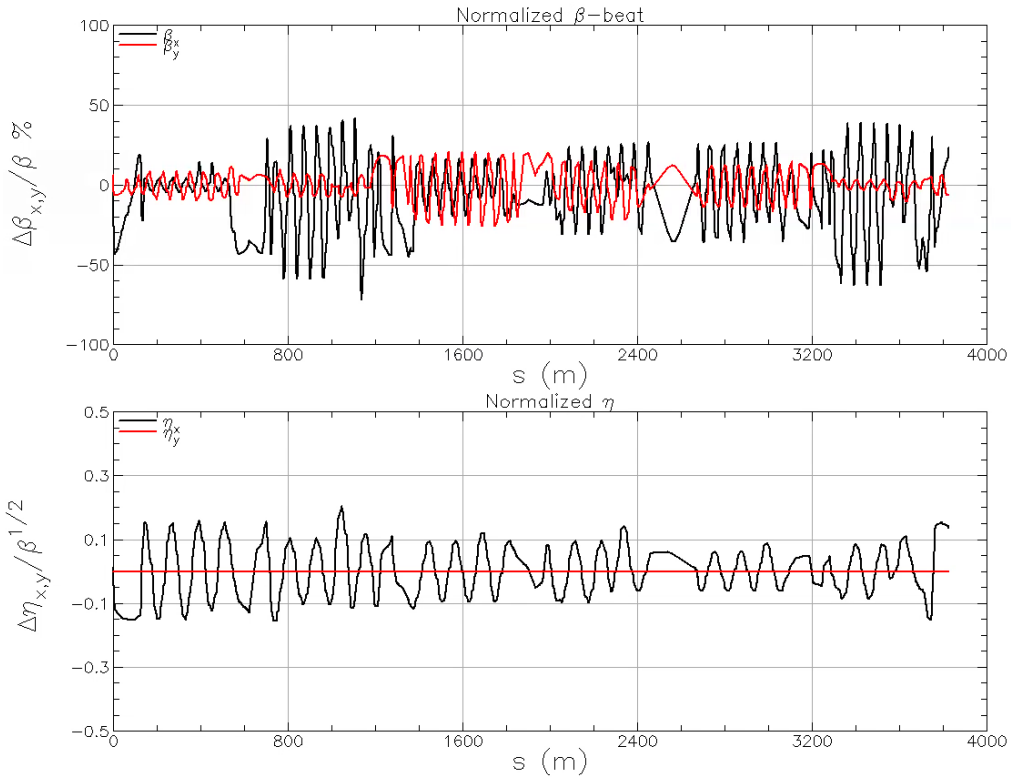


(c)

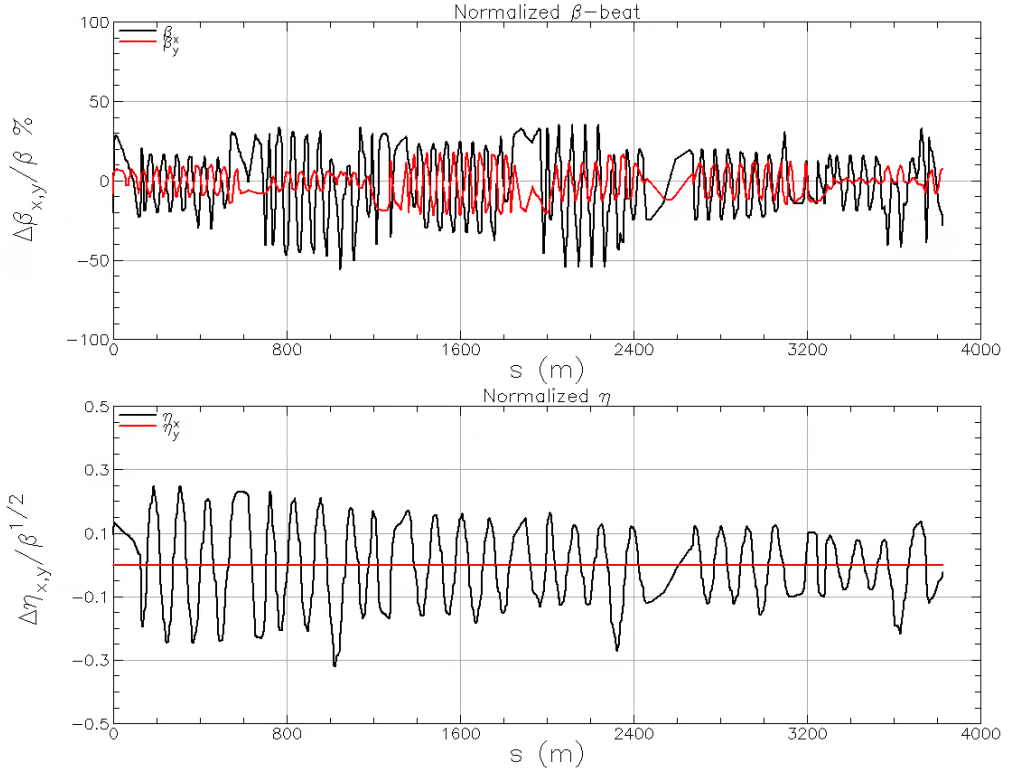


(d)

Figure 8: The evolution of the $\Delta Q_{h,v}$ (Fig. 8a), $\beta_{max\,x,y}$ (Fig. 8b), $\Delta\gamma_T$ (Fig. 8c), and $\eta_{max\,x,y}$ (Fig. 8d).



(a) The pre-jump wave generation. Top: β-wave with black curve horizontal and red vertical wave. Bottom: β-wave with black curve horizontal and red vertical wave.



(b) The post-jump wave generation. Top: β-wave with black curve horizontal and red vertical wave. Bottom: β-wave with black curve horizontal and red vertical wave.

Figure 9: The wave generation during the transition jump of the G24Q20 cooling configuration.

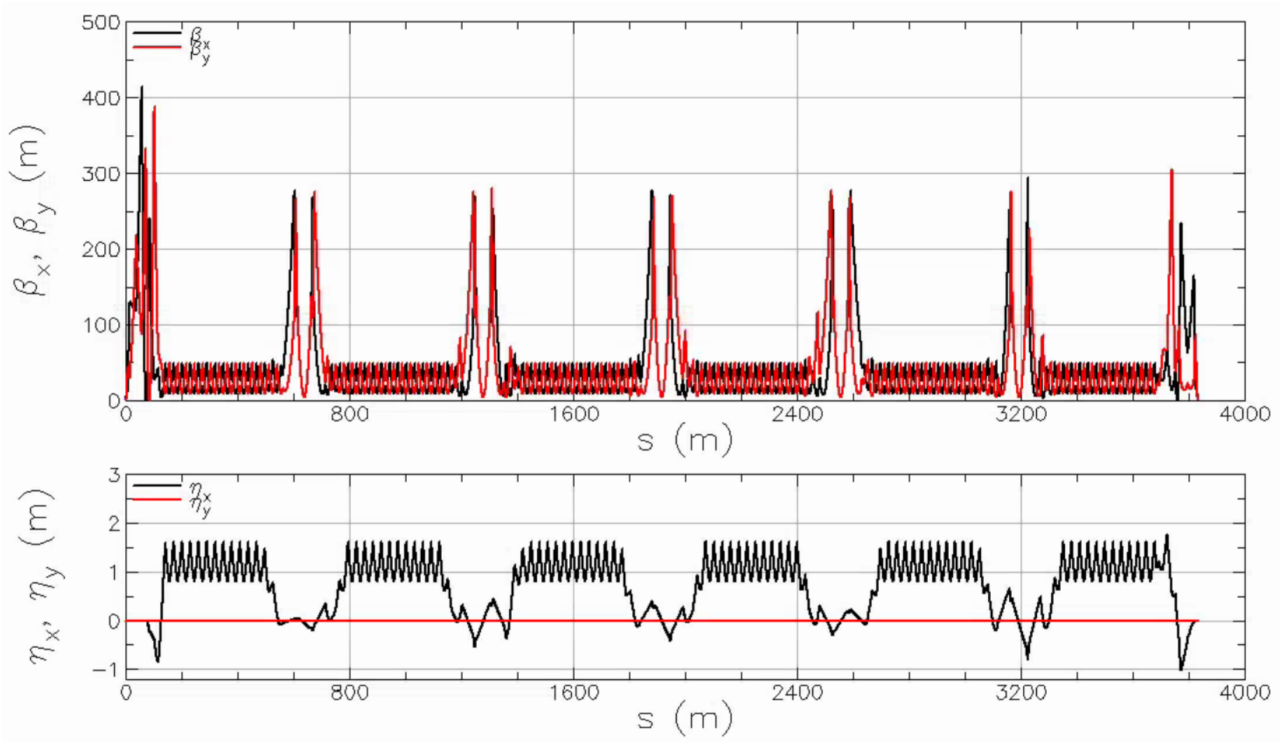


Figure 10: The HSR transition optics with a RHIC-like IR2 layout (#e74404c) starting at IP6 with increasing s clockwise. The beam direction is from right to left in the two plots. Top: Twiss parameters with black the horizontal plane and red the vertical plane. Bottom: Dispersion with black the horizontal plane and red the vertical plane.

of the jump quadrupoles at peak excitation are in Tab. 5.

Jump Quadrupole PS	Current (A)
GTI	32
QTI	34
GTO	22
QTO	45

Table 5: The power supply absolute value of the peak current for G24Q20-nocool transition jump configuration. The current has been rounded to the nearest amp.

Configuration	**G24Q20-noir6-Pre**	**G24Q24-ir6-Pre**	**G24Q20-noir6-Post**	**G24Q24-ir6-Post**
Hor. β-wave RMS	0.1600	0.1505	0.1319	0.1400
Ver. β-wave RMS	0.0584	0.0557	0.0574	0.0533
Hor. η-wave RMS $\sqrt{m}$	0.0893	0.0814	0.1478	0.1516

Table 6: β- and η-wave RMS values for the RHIC-like IR2 lattice layout.

3.4 HSR with G24Q24-nocool Configuration (RHIC-like IR2)

If the HSR maintains the non-cooling IR2 and if four jump quadrupoles are available in IR6, the FOM G24Q24-nocool configuration can be restored. The challenge is that in IR6 the phase advance and dispersion vary from

what is designed in the other IRs which will have an adverse effect on the mitigation of the β and η-wave generation. The current design, after optimization, shows that only the IR6 jump quadrupoles is effective when jumping transition. Figure 12 shows the β and η-wave generation which does not show a significant reduction in wave generation when compared to Fig. 11. This is also clearly shown in the comparison table, Tab. 6, where the RMS values are nearly equal. Table 7 are the currents for the jump quadrupoles at peak excitation before the jump. The

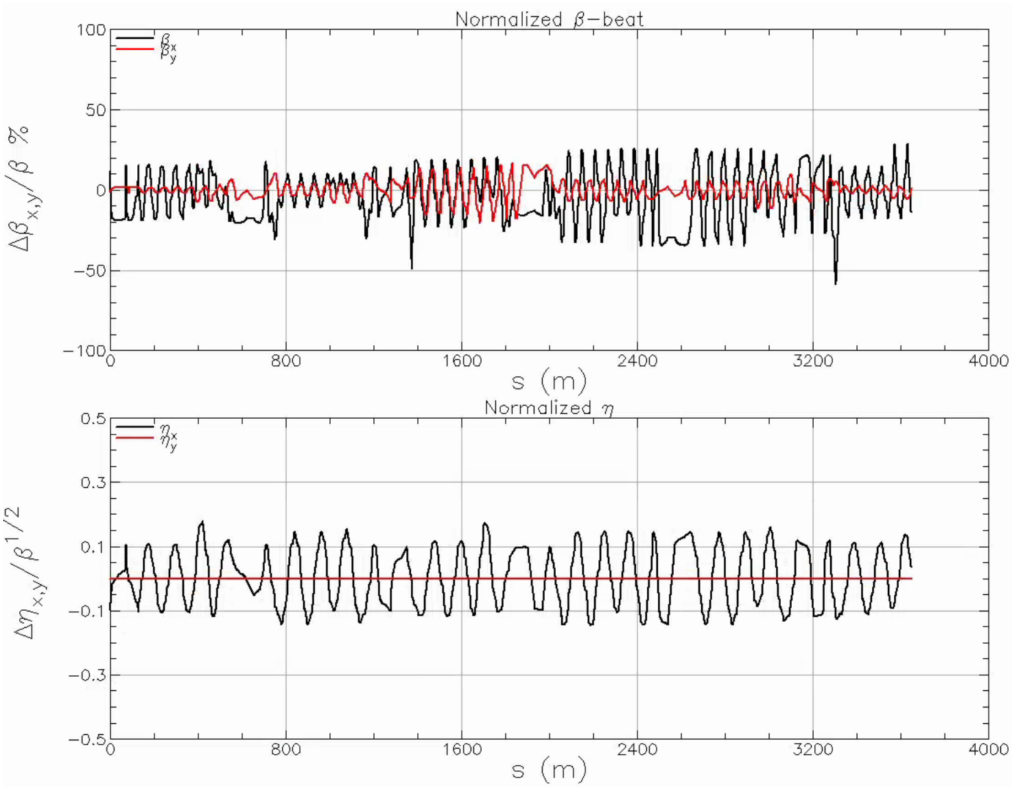
Jump Quadrupole PS	Current (A)
GTI	32
QTI	33
GTO	23
QTO	46
QTR10	8

Table 7: The power supply absolute value of the peak current for G24Q24-nocool transition jump configuration. The current has been rounded to the nearest amp.

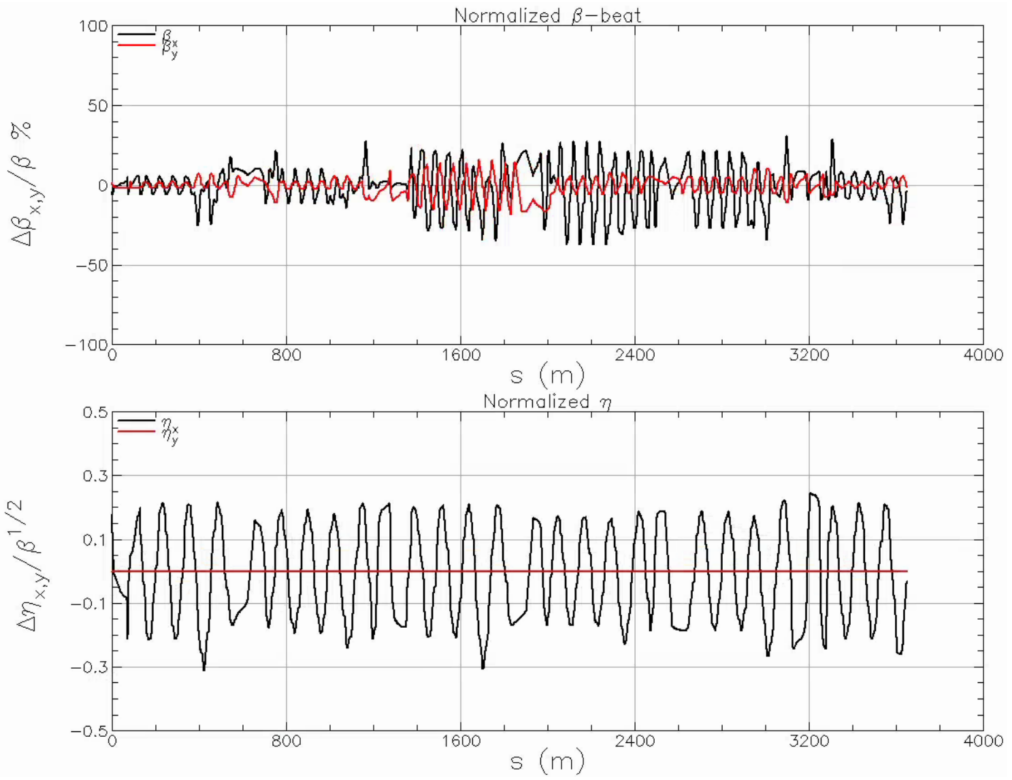
effectiveness of the QTR10, the jump quadrupole on the incoming side IR6, jump quadrupole is a result of the horizontal β-function having an amplitude of 44.7 m which is within 3% of the average β-function of the RHIC-like IRs.

4 Conclusion

The HSR transition jump scheme for the cooling lattice was presented. The configurations G24Q16-cool and G24Q20-cool were compared through the wave generation when the jump quadrupoles are excited. The RMS value for the pre-jump G24Q16-cool β-wave is 40% larger than the G24Q20-cool configuration but more importantly the horizontal tune shift is 0.02 in the G24Q16-cool configuration which has a greater chance of landing on a tune resonance when jumping transition. If the HSR has the no cooling IR2 for the first year of physics collisions, the G24Q20-nocool and G24Q24-nocool configurations of the lattice are comparable.

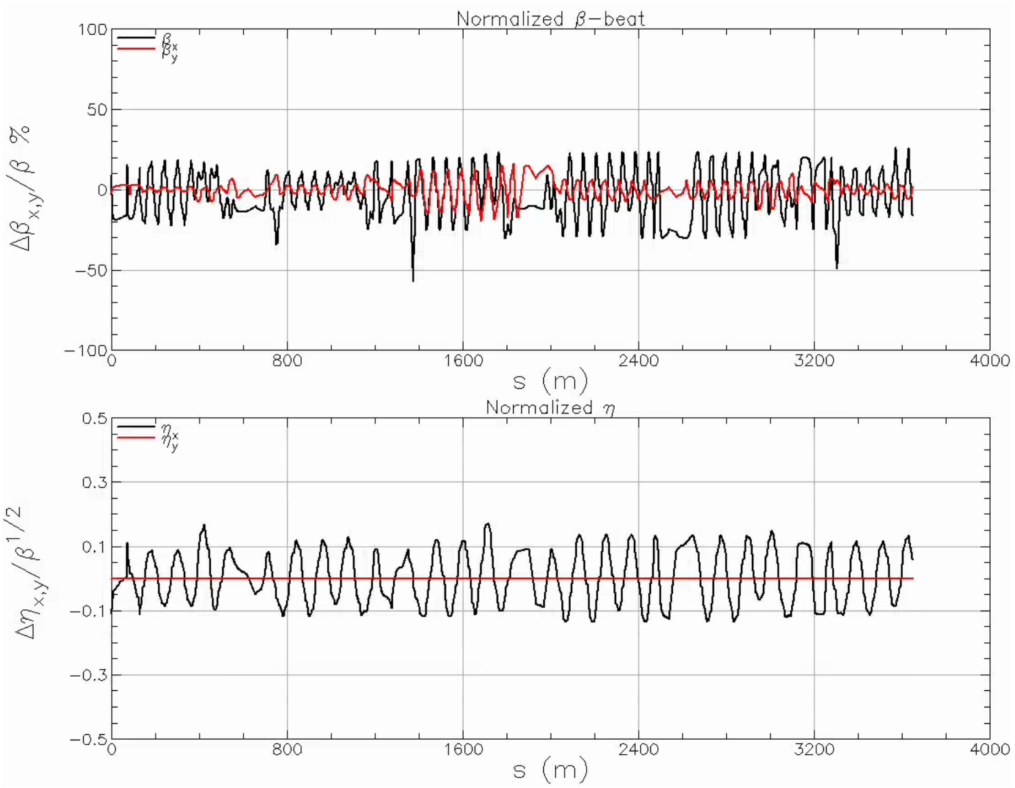


(a) The pre-jump wave generation. Top: β-wave with black curve horizontal and red vertical wave. Bottom: β-wave with black curve horizontal and red vertical wave.

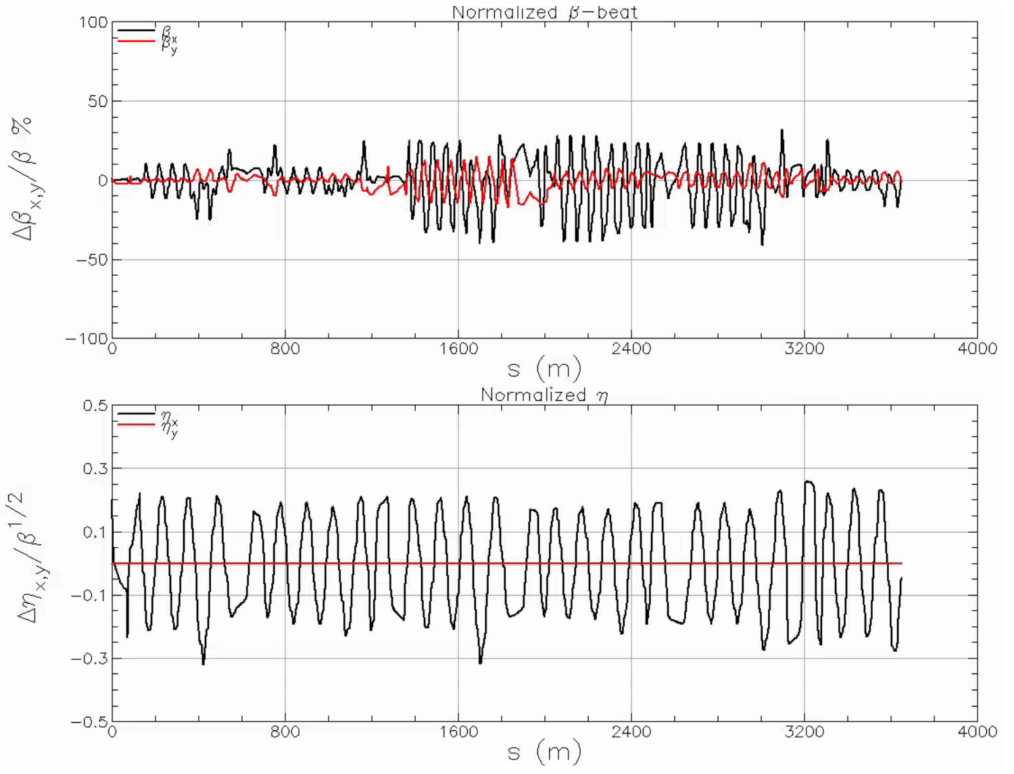


(b) The post-jump wave generation. Top: β-wave with black curve horizontal and red vertical wave. Bottom: β-wave with black curve horizontal and red vertical wave.

Figure 11: The wave generation during the transition jump for the G24Q20-nocool configuration without cooling.

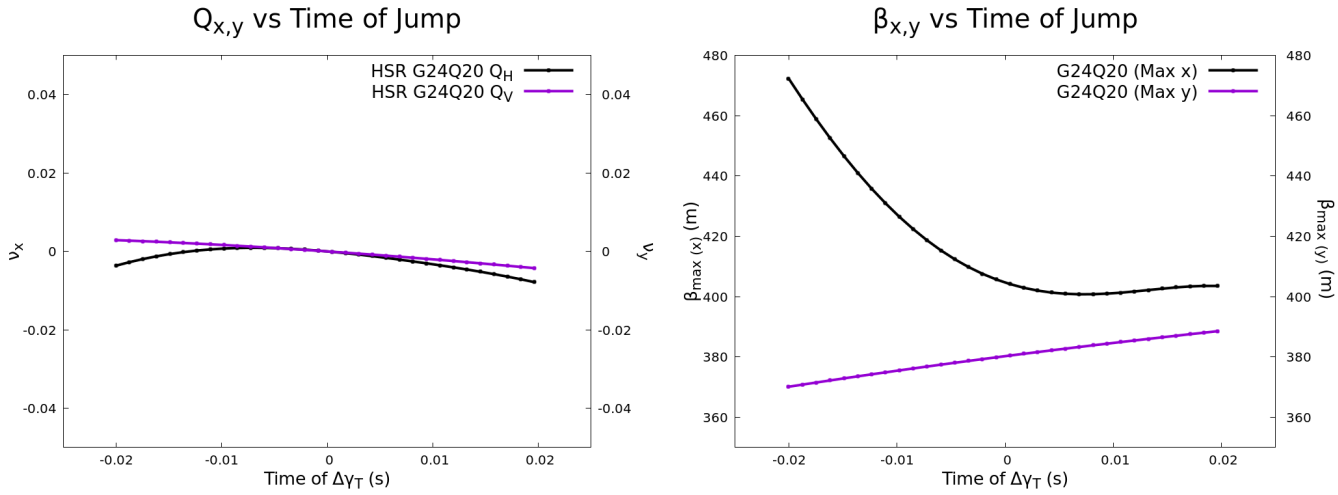


(a) The pre-jump wave generation. Top: β-wave with black curve horizontal and red vertical wave. Bottom: β-wave with black curve horizontal and red vertical wave.



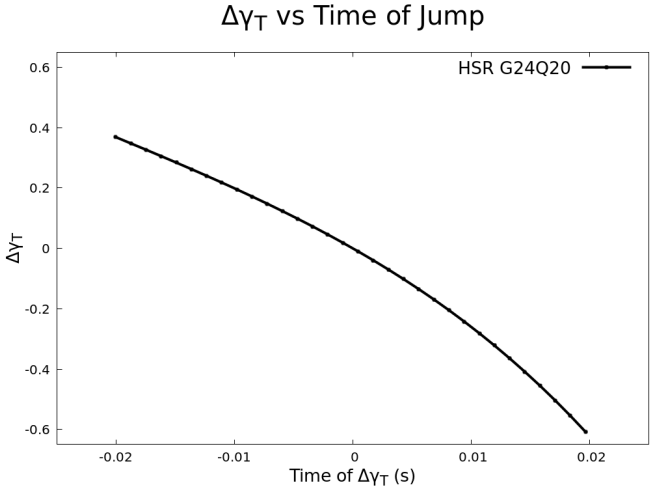
(b) The post-jump wave generation. Top: β-wave with black curve horizontal and red vertical wave. Bottom: β-wave with black curve horizontal and red vertical wave.

Figure 12: The wave generation during the transition jump for the G24Q24 configuration without cooling.

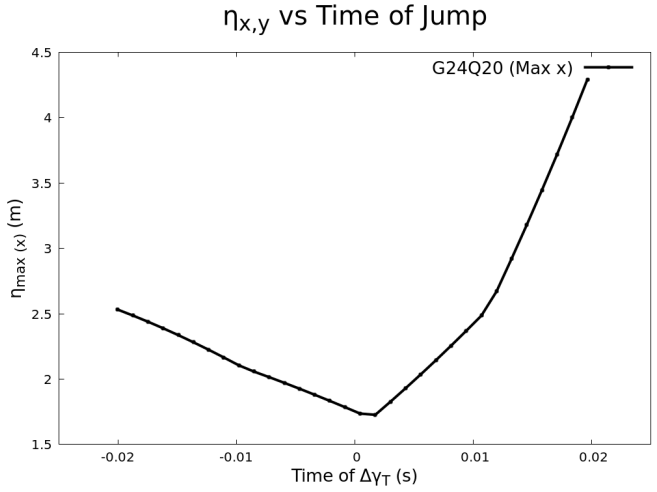


(a)

(b)



(c)



(d)

Figure 13: The evolution of the $\Delta Q_{h,v}$ (Fig. 13a), $\beta_{max\,x,y}$ (Fig. 13b), $\Delta\gamma_T$ (Fig. 13c), and $\eta_{max\,x,y}$ (Fig. 13d).

Inner Power supply index p	Power supply name	Quad name	Sensitivities Quad Individual		Sensitivities PS G family		Sensitivities PS Q family		Sensitivities Quad Individual		Sensitivities PS G family		Sensitivities PS Q family	
			S_Q	S_G	S_Q	S_G	S_Q	S_G	S_{bw}	S_{hw}	S_{bw}	S_{hw}	S_{bw}	S_{hw}
			m	m	m	m	m	m	m	$m\sqrt{m}$	m	m	m	m
2	yi2_qgt_ps	yi2_qgt5	0.00	0.00			8.26	0.73	0.00	0.00			-3.72	0.55
		yi2_qgt7	0.00	0.00					0.00	0.00				
		yi3_qgt5	4.27	0.04					21.34	0.69				
		yi3_qgt7	3.99	0.70					-25.06	-0.14				
3	yi3_qgt_ps	yi3_qgt11	3.53	4.58	14.13	18.34			-17.41	2.49	-3.27	-1.01		
		yi3_qgt13	3.53	4.58					15.92	-6.97				
		yi3_qgt15	3.53	4.58					-14.31	-3.18				
		yi3_qgt17	3.53	4.59					12.53	6.66				
6	yi6_qgt_ps	yi6_qgt5	0.00	0.00			8.62	0.59	0.00	0.00			-21.12	-0.44
		yi6_qgt7	0.00	0.00					0.00	0.00				
		yi7_qgt5	4.77	0.00					2.02	-0.01				
		yi7_qgt7	3.85	0.59					-23.14	-0.43				
7	yi7_qgt_ps	yi7_qgt11	3.53	4.58	14.13	18.34			-21.75	-0.81	-1.57	0.89		
		yi7_qgt13	3.53	4.58					21.17	7.43				
		yi7_qgt15	3.53	4.59					-20.38	1.55				
		yi7_qgt17	3.53	4.59					19.39	-7.28				
10	yi10_qgt_ps	yi10_qgt5	4.34	0.07			17.24	1.49	17.95	-0.93			31.16	-1.22
		yi10_qgt7	4.07	0.77					-2.21	2.23				
		yi11_qgt5	4.97	0.02					-6.99	0.35				
		yi11_qgt7	3.86	0.64					22.42	-2.87				
11	yi11_qgt_ps	yi11_qgt11	3.53	4.58	14.13	18.34			21.97	7.50	1.27	-0.64		
		yi11_qgt13	3.54	4.58					-21.55	0.96				
		yi11_qgt15	3.53	4.58					20.85	-7.41				
		yi11_qgt17	3.54	4.58					-20.00	-1.70				
Outer Power supply index p	Power supply name	Quad name	Individual		G family		Q family		Individual		G family		Q family	
			S_Q	S_G	S_Q	S_G	S_Q	S_G	S_{bw}	S_{hw}	S_{bw}	S_{hw}	S_{bw}	S_{hw}
			m	m	m	m	m	m	m	$m\sqrt{m}$	m	m	m	m
1	yo1_qgt_ps	yo1_qgt12	3.72	4.80	14.89	19.19			-19.56	2.28	-2.83	-0.94		
		yo1_qgt14	3.72	4.80					18.29	-7.46				
		yo1_qgt16	3.72	4.80					-16.91	-2.95				
		yo1_qgt18	3.72	4.80					15.35	7.19				
4	yo4_qgt_ps	yo4_qgt6	3.10	0.03			6.86	1.50	4.11	0.41			9.06	3.83
		yo4_qgt8	3.76	1.47					4.95	3.42				
		yo5_qgt6	0.00	0.00					0.00	0.00				
		yo5_qgt8	0.00	0.00					0.00	0.00				
5	yo5_qgt_ps	yo5_qgt12	3.72	4.80	14.89	19.19			-22.92	0.84	-1.46	-0.84		
		yo5_qgt14	3.72	4.80					22.37	-7.81				
		yo5_qgt16	3.72	4.80					-21.65	-1.55				
		yo5_qgt18	3.72	4.80					20.74	7.68				
8	yo8_qgt_ps	yo8_qgt6	3.28	0.02			14.00	2.97	5.83	0.42			-2.21	-5.78
		yo8_qgt8	3.61	1.34					-16.25	-1.55				
		yo9_qgt6	3.09	0.01					-12.81	-0.12				
		yo9_qgt8	4.02	1.60					21.02	-4.54				
9	yo9_qgt_ps	yo8_qgt6	3.72	4.80	14.89	19.19			22.14	7.79	-0.86	-0.80		
		yo8_qgt8	3.72	4.80					-22.76	-0.97				
		yo9_qgt6	3.72	4.80					23.17	-7.88				
		yo9_qgt8	3.72	4.80					-23.41	0.25				
12	yo12_qgt_ps	yo12_qgt6	3.25	0.00			6.88	1.37	9.20	0.19			6.22	2.93
		yo12_qgt8	3.63	1.36					-2.99	2.74				
		yo1_qgt6	0.00	0.00					0.00	0.00				
		yo1_qgt8	0.00	0.00					0.00	0.00				

Table 8: The tune and wave sensitivities based on an 87° phase advance per cell lattice. The missing jump quadrupoles when compared to RHIC are in red font. The inner power supply configuration strength ratios are $k_{inner} = -1.24$ and the outer $k_{outer} = -1.61$

Inner Power supply index p	Power supply name	Quad name	Sensitivities, quad PREDICTED		Sensitivities PS, THEORY G family		Q family		Sensitivities, quad PREDICTED		Sensitivities PS, THEORY G family		Q family	
			S_Q	S_G	S_Q	S_G	S_Q	S_G	S_{bw}	S_{hw}	S_{bw}	S_{hw}	S_{bw}	S_{hw}
			m	m	m	m	m	m	m	$m\sqrt{m}$	m	m	m	m
2	yi2_qgt_ps	yi2_qgt5	3.54	0.01			15.72	1.61	20.71	0.33			19.04	1.63
		yi2_qgt7	4.25	0.63					-6.02	-1.91				
		yi3_qgt5	3.94	0.07					-20.17	-0.31				
		yi3_qgt7	4.00	0.89					24.53	3.51				
3	yi3_qgt_ps	yi3_qgt11	3.55	4.58	14.19	18.32			20.09	-7.34	2.32	0.49		
		yi3_qgt13	3.55	4.58					-19.09	-2.04				
		yi3_qgt15	3.55	4.58					17.91	7.16				
		yi3_qgt17	3.55	4.58					-16.59	2.71				
6	yi6_qgt_ps	yi6_qgt5	0.00	0.00			7.41	1.02	0.00	0.00			-12.55	2.11
		yi6_qgt7	0.00	0.00					0.00	0.00				
		yi7_qgt5	3.48	0.01					0.51	0.30				
		yi7_qgt7	3.93	1.00					-13.06	1.81				
7	yi7_qgt_ps	yi7_qgt11	3.55	4.58	14.19	18.32			-21.57	-1.00	0.53	-0.67		
		yi7_qgt13	3.55	4.58					22.03	-7.51				
		yi7_qgt15	3.55	4.58					-22.29	0.29				
		yi7_qgt17	3.55	4.58					22.36	7.54				
10	yi10_qgt_ps	yi10_qgt5	3.39	0.22			16.52	3.20	10.19	1.39			-6.54	7.66
		yi10_qgt7	4.55	2.34					4.94	4.68				
		yi11_qgt5	4.58	0.03					**-4.69**	**0.41**				
		yi11_qgt7	4.00	0.61					-16.98	1.18				
11	yi11_qgt_ps	yi11_qgt11	3.55	4.58	14.19	18.32			-21.28	-1.17	0.71	-0.65		
		yi11_qgt13	3.55	4.57					21.83	-7.49				
		yi11_qgt15	3.55	4.58					-22.18	0.47				
		yi11_qgt17	3.55	4.59					22.35	7.55				
Outer Power supply index p	**Power supply name**	**Quad name**	**PREDICTED**		**G family**		**Q family**		**PREDICTED**		**G family**		**Q family**	
			S_Q	S_G	S_Q	S_G	S_Q	S_G	S_{bw}	S_{hw}	S_{bw}	S_{hw}	S_{bw}	S_{hw}
			m	m	m	m	m	m	m	$m\sqrt{m}$	m	m	m	m
1	yo1_qgt_ps	yo1_qgt12	3.74	4.79	14.95	19.18			23.25	-7.89	1.11	0.59		
		yo1_qgt14	3.74	4.79					-22.86	-0.96				
		yo1_qgt16	3.74	4.80					22.29	7.82				
		yo1_qgt18	3.74	4.80					-21.58	1.62				
4	yo4_qgt_ps	yo4_qgt6	3.23	0.04			6.92	1.43	-13.86	-0.25			-0.78	3.49
		yo4_qgt8	3.69	1.39					13.07	3.75				
		yo5_qgt6	0.00	0.00					0.00	0.00				
		yo5_qgt8	0.00	0.00					0.00	0.00				
5	yo5_qgt_ps	yo5_qgt12	3.74	4.79	14.95	19.18			-23.47	-0.34	-0.17	-0.69		
		yo5_qgt14	3.74	4.79					23.55	-7.92				
		yo5_qgt16	3.74	4.80					-23.47	-0.33				
		yo5_qgt18	3.74	4.80					23.22	7.90				
8	yo8_qgt_ps	yo8_qgt6	3.48	0.01			14.16	2.62	21.48	-0.29			7.91	2.55
		yo8_qgt8	3.52	1.25					-21.51	-0.48				
		yo9_qgt6	3.40	0.00					5.02	0.15				
		yo9_qgt8	3.77	1.36					2.92	3.18				
9	yo9_qgt_ps	yo8_qgt6	3.74	4.79	14.95	19.18			7.09	-6.38	-3.60	0.95		
		yo8_qgt8	3.74	4.79					-8.96	4.41				
		yo9_qgt6	3.74	4.80					10.77	6.77				
		yo9_qgt8	3.74	4.80					-12.50	-3.84				
12	yo12_qgt_ps	yo12_qgt6	3.25	0.00			13.78	2.86	9.20	0.19			0.37	5.38
		yo12_qgt8	3.63	1.36					-2.99	2.74				
		yo1_qgt6	3.09	0.00					1.82	-0.15				
		yo1_qgt8	3.80	1.49					-7.67	2.60				

Table 9: The tune and wave sensitivities based on an 87° phase advance per cell lattice and non-cooling IR2. The missing jump quadrupoles when compared to RHIC are in red font. The inner power supply configuration strength ratios are $k_{inner} = -1.07$ and the outer $k_{outer} = -1.29$

References

[1] S. Peggs, A. Drees, H. Lovelace III, and G. Robert-Demolaize, "Hsr transition jump optics in the september 2022 layout," Tech. Rep. EIC-ADD-TN-41, Brookhaven National Laboratory, 3 2023.

[2] Accelerator Division, *RHIC: Relativistic Heavy Ion Collider Configuration Manual*. Collider-Accelerator Department, Upton,NY, 4 ed., November 2006.

[3] A. Sørensen, "Crossing The Phase Transition In Strong Focusing Proton synchrotrons," *Part. Accel.*, vol. 6, pp. 141–165, 1975.

[4] J.-P. Burnet, C. Carli, M. Chanel, R. Garoby, S. Gilardoni, M. Giovannozzi, S. Hancock, H. Haseroth, K. Hübner, D. Küchler, J. Lewis, A. Lombardi, D. Manglunki, M. Martini, S. Maury, E. Métral, D. Möhl, G. Plass, L. Rinolfi, R. Scrivens, R. Steerenberg, C. Steinbach, M. Vretenar, and T. Zickler, *Fifty years of the CERN Proton Synchrotron: Volume 1*. CERN Yellow Reports: Monographs, Geneva: CERN, 2011.

[5] S. Koscielniak, "Near-Adiabatic Capture of Pendulum Phase Space," Tech. Rep. TRI-BN-23-10, TRIUMF, Vancouver, BC, Canada, 2023.

[6] K. Johnsen, "Effects Of Non-Linearities On The Phase Transition," in *CERN Symposium on High-Energy Accelerators and Pion Physics*, vol. 1, pp. 106–111, 1956.

[7] S. Peggs, S. Tepikian, and D. Trbojevic, "A First Order Matched Transition Jump at RHIC," in *Proceedings of International Conference on Particle Accelerators*, pp. 168–170 vol.1, 1993.

[8] J. Wei, "Transition Crossing in the RHIC," 1 1992.

[9] Peggs, S. and Wei, J., "Longitudinal Phase Space Parameters," 7 1996.

[10] A. W. Chao, K. H. Mess, M. Tigner, and F. Zimmermann, *Handbook of Accelerator Physics and Engineering*. WORLD SCIENTIFIC, 2nd ed., 2013.

[11] M. Harrison, S. Peggs, and T. Roser, "The RHIC Accelerator," *Annual Review of Nuclear and Particle Science*, vol. 52, no. 1, pp. 425–469, 2002.

[12] H. Lovelace III, J. S. Berg, S. Peggs, S. Polizzo, V. Ptitsyn, and G. Robert-Demolaize, "Transition Jump System of the Hadron Storage Ring of the Electron Ion Collider," *JACoW*, vol. IPAC2023, p. MOPA056, 2023.